BSc Thesis Applied Physics - Applied Mathematics

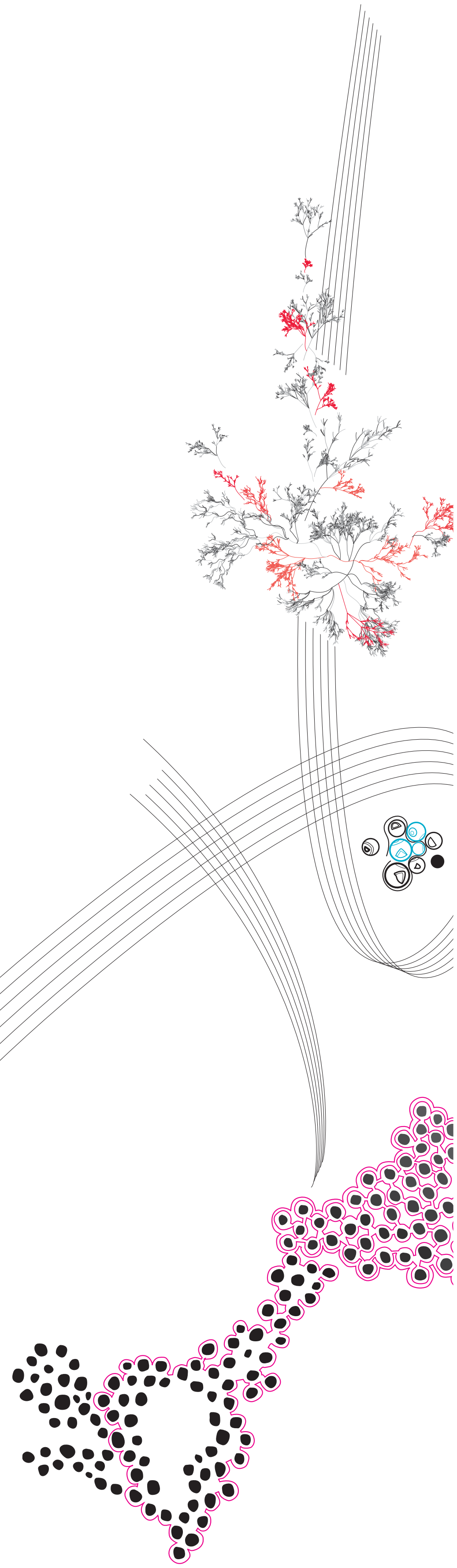

Quantum Mechanical Modelling of Carbon Nanotube Transistor

Willem Haklander

Supervisors:
prof.dr. Gerard H.L.A. Brocks
prof.dr.ir. Bernard J. Geurts

Second examinors:
prof.dr.ir. Alexander Brinkman
prof.dr.ir. Frederic Schuller

July, 2020

Chair of Multiscale Modeling and Simulation (MMS)
Faculty of Electrical Engineering,
Mathematics and Computer Science

Chair of Quantum Transport in Matter (QTM)
Faculty of Science and Technology

UNIVERSITY OF TWENTE.

Preface

I thank Bernard and Geert for the helpful weekly discussions, their guidance in choosing the right priorities concerning the thesis and their feedback in the different stages of my work.

Quantum Mechanical Modelling of Carbon Nanotube Transistor

Willem Haklander*

July, 2020

Abstract

Transistor sizes produced by the semiconductor industry have by now reached the sub-10 nanometer range. One type of nanoscale transistors currently under heavy research is the carbon nanotube, a rolled-up version of graphene. In this paper, the quantum mechanical treatment of electronic transport in a nanotube transistor is described. Results from quantum mechanics, solid-state physics, electrostatics and numerical analysis are combined into a computer model to obtain a self-consistent solution. Simulations are run which demonstrate the validity of the model. *Keywords*: Carbon nanotube transistor, Electronic transport, Tight-binding method, Non-equilibrium Green's function, Poisson's equation

1 Introduction

The constant trend in the semiconductor industry of a two-yearly doubling of the transistor density on integrated circuits was predicted by Gordon Moore already in 1975[8]. By now, transistor sizes have reached the sub-10 nanometer scale, posing a whole new range of difficulties to overcome[9]. Transistors built from carbon nanotubes, a rolled-up version of graphene, show promising results concerning their performance and scalability[10]. This report describes the thinking and working process behind the modelling of such a carbon nanotube transistor (CNT).

1.1 Description of the model

A common approach to modelling electronic nanoscale devices is by building a Schrödinger-Poisson solver. Such a model consists of two "blocks": one which solves the Schrödinger equation and one which solves the Poisson equation for the specific device. The simulation alternates between block 1 and block 2, using the output of one block as the input of the other block. This is repeated until a self-consistent solution is reached, from which the desired physical properties can be calculated. The model in this report uses a similar approach, but instead of Schrödinger's equation the equivalent Green's function is solved for the device. This provides an easier way of incorporating the boundary conditions for this device, as will be explained in section 4. The procedure of the model is given and explained in figure 1.

---

*Email: w.haklander@student.utwente.nl

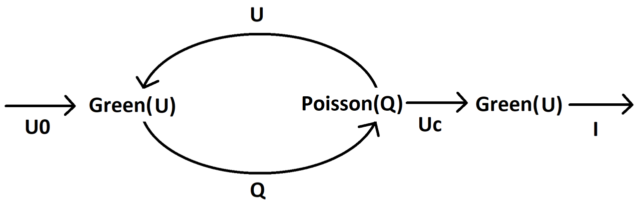

FIGURE 1: The procedure of the final program. After quessing an initial potential $U_0(x)$, the electron charge $Q_e(x)$ and the potential $U(x)$ are calculated iteratively using the Green's function formalism and the Poisson solver. After self-consistency is reached, the final potential $U_c(x)$ is used to calculate the current flowing through the device.

1.2 Structure of the document

This document is composed of a cover page, a preface, a document body divided into eight sections and a list of references. These are the names of the different sections and their respective aims:

1. **Introduction** Gives the basic motivation for the paper, the modelling approach and the outline of the document.

2. **The Carbon Nanotube Transistor** Introduces the reader to the modelled device in this research effort. Breaks down the device into the keywords *Carbon*, *Nanotube* and *Transistor* and points out the relevant aspects they entail.

3. **Schrödinger's Equation and the Tight-Binding Method** The beginning of the theoretical part of the paper (which spans from section 3 to 5) which introduces the quantum-mechanical description of electrons in the device. Uses the tight-binding approximation and Bloch orbitals to set up the Hamiltonian matrix equation required to be solved in the model.

4. **The Non-Equilibrium Green's Function Method** Motivates the introduction of the Green's function formalism for solving the problem in section 3. Derives the matrix form of the Green's function and the self-energies which it contains. Gives formulas for destillating the charge density and the electric current from the Green's function and the self-energies.

5. **The Poisson Equation** Gives the second part of the model next to the Green's function method, solving the Poisson equation in electrostatics for the cylindrical geometry of the device. Defines the complete problem with its boundary conditions first analytically. Uses Gauss' law, a two-dimensional grid and the finite-difference method to discretise the problem into a five-diagonal matrix equation.

6. **Results** Shows the results of the final model which support the convergence of the model and the validity of the model. Gives characteristics of the CNT which illustrate the applicability of the device as a transistor.

7. **Discussion** Looks back at several difficulties in the building process of the model and possible flaws it has. Discusses possible ways how the speed and the performance of the model could be improved and gives inspiration for how the model could be applied to find an optimal version of the CNT.

8. **Appendices** Contains the lengthy and less interesting derivations of the electron wavefunction basis from section 3, the self-energies and the surface Green's functions from section 4 and the matrix equation for the Poisson problem from section 5.

2 The Carbon Nanotube Transistor

The aim of this section is to get the reader more familiar with the modelled device. First, attention will be given to carbon and its two-dimensional hexagonal lattice form, graphene.

2.1 Carbon

The electron configuration of an isolated carbon atom is $1s^2 2s^2 2p^2$. The two $1s$ states are confined to the nucleus and do not take part in binding the atom. The $2s$ and $2p$ states, four in total, can form so-called sp^2 bonds. With all carbon atoms in one plane, each atom are then bound to 3 other atoms, making 120 degree angles with each other to form the hexagonal lattice called *graphene*. Figure 2 shows such a hexagon inside graphene.

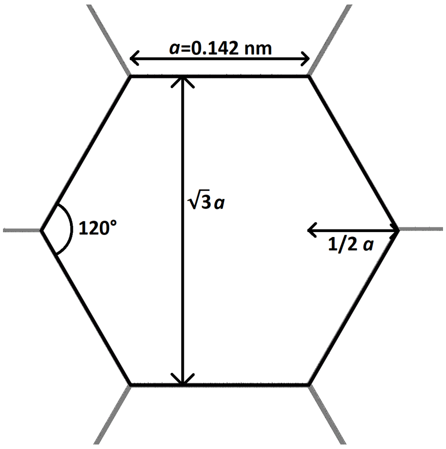

Figure 2: The hexagonal structure formed by carbon atoms inside a graphene lattice, with the carbon-carbon distance $a = 0.142$ nm[6]

.

When defining the graphene plane as the x-y plane, at each atom the p_x and p_y orbitals are involved in the sp^2 bonds while the p_z orbital perpendicular to the graphene plane remains free.[1] An infinite graphene plane is a zero-gap semiconductor and a very good electric conductor. More precisely, electrons inside graphene have negligible electric resistivity caused by scattering. By confining the length of the plane in one direction, the band structure can be altered to have a non-zero band gap, as will be shown in the rest of this section.

2.2 Nanotube

It is possible to manipulate a rectangular piece of graphene like shown in figure 3a) to form a carbon-based hollow cylinder. For a tube with a diameter in the range of nanometers, the structure is called a (single-walled) carbon nanotube (CN). CNs can be either metallic or semiconducting[6]. In this report a semiconducting $(13, 0)$ zig-zag nanotube (following the standard (n, m)-notation for CNs) is modelled, consisting of $N = 100$ rings of each $M = 13$ atoms. In a zig-zag type nanotube a distinction can be made between two kinds of rings, A and B, as in figure 3b).

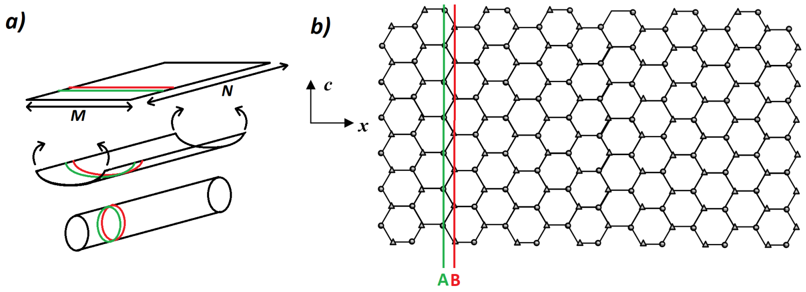

FIGURE 3: *a)* The formation of a carbon nanotube out of graphene, having M atoms in the circumferential and N in the longitudional direction. *b)* The two kinds of rings, A and B, inside a zig-zag nanotube. *Source original figure: [6]*

The radius r of this CN is approximately

$$r = \frac{M\sqrt{3}a}{2\pi} = 0.51 \text{ nm} \tag{1}$$

and the length is

$$L = \frac{N}{2}\frac{a}{2} + \left(\frac{N}{2} - 1\right)a = 10.5 \text{ nm}. \tag{2}$$

The bandgap of this nanotube is non-zero:

$$E_g = 0.82 \text{ eV}, \tag{3}$$

as will also be derived in section 3.

2.3 Transistor

Figure 4 gives the layout of the CNT.

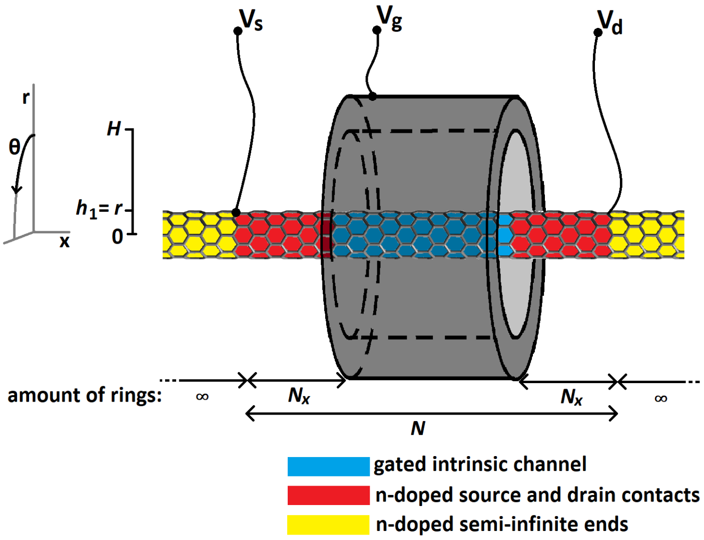

FIGURE 4: The carbon nanotube transistor consisting of the nanotube and the gate, together with its cylindrical coordinate system. *Source original figure: [4]*

The simulated area, i.e. the "device", is the middle section of figure 4 of N rings wide. The effect of the yellow semi-infinite ends on the device is calculated and added using the Green's function formalism.

A potential difference is fixed between the two contacts and a metallic gate influences the potential to the channel, controlling the current flow from the source to the drain. The contacts as well as the semi-infinite ends are uniformly n-type doped with doping concentration n_d, which results in a Fermi level shift of E_d. This setup is comparable to (N^+–I–N^+) type metal–oxide–semiconductor field-effect transistors (MOSFETs). Figure 5 shows the bandstructure of different configurations of the CNT, containing the following energy levels:

1. μ the Fermi level, also called the chemical potential.
2. E_c the conduction band level.
3. E_v the valence band level.
4. U the electrochemical potential, which is equal to the chemical potential plus the electrostatic potential.
5. E_d the energy level shift of the Fermi level because of doping.

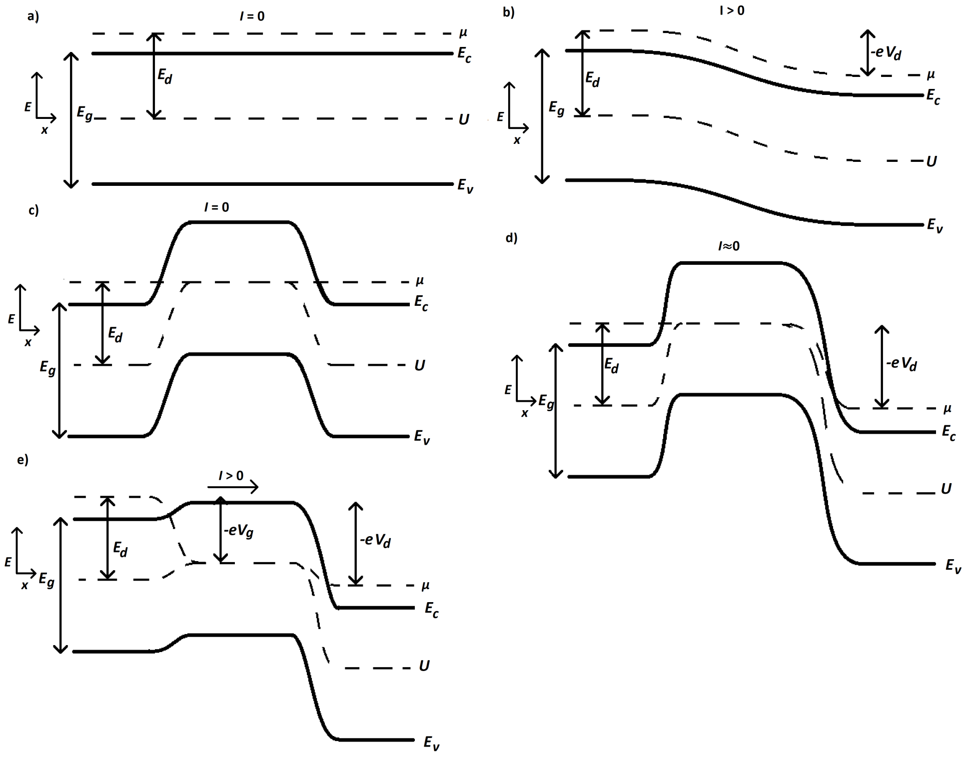

FIGURE 5: Bandstructure of the CNT with *a)* uniform n-doping, *b)* uniform doping with applied drain voltage, *c)* (N^+-I-N^+) doping (n-doped source and drain contacts and intrinsic (undoped) channel), *d)* (N^+-I-N^+) doping and applied drain voltage, *e)* (N^+-I-N^+) doping and applied gate and drain voltages.

The local density of states distributions of the source and drain contacts are filled up to the source and drain Fermi levels E_{FS} and E_{FD}, respectively. At energy levels where there are both occupied and unoccupied states, electrons (and holes) are able to jump between states. In this context, this implies that only electrons lying inside the energy range $E_{FD} \leq E \leq E_{FS}$ are able to contribute to the current. In a), no current flows, since the device is in equilibrium, i.e. $E_{FS} = E_{FD}$. In b), applying a positive voltage to the drain while the source is kept at 0V, electrons within the energy window will move from the source to the drain, which means that the current is nonzero. In c), an undoped channel is added between the source and drain. A positive drain voltage will now result in almost no current, as shown in d). This occurs because the electrons cannot pass through the channel, where the energy window lies within the bandgap which has a very low DOS. When the gate voltage, which alters the potential inside the channel, is increased, the channel conduction band is lowered with respect to the source and drain. When the conduction band falls within the two Fermi levels, the current from source and drain is increased exponentially. This "on-off" switching behavior is characteristic for MOSFETs and the main goal of the model is to reproduce the I-V characteristic which shows this behavior.

3 Schrödinger's Equation and the Tight-Binding Method

In the previous section the modelled device was defined to consist of $N = 100$ rings of each $M = 13$ atoms. The charge distribution inside this device is treated quantum-mechanically. This means that the total electron distribution of the device is represented with a wavefunction $\Psi(\mathbf{r})$ which obeys the time-independent Schrödinger equation

$$\hat{H}\Psi(\mathbf{r}) = \Big[\frac{-\hbar^2}{2m}\nabla^2 + U(\mathbf{r})\Big]\Psi(\mathbf{r}) = E\Psi(\mathbf{r}). \tag{4}$$

The Hamiltonian operator $\hat{H}$ consists of the Laplace operator ∇^2 and the electrostatic potential $U(\mathbf{r})$. In this section, the problem of solving equation 4 for the $N \times M$ graphene lattice will be transformed into the problem of solving M matrix-vector eigenvalue equations with matrix size $N \times N$. For this, the tight-binding model and Bloch orbitals will be introduced.

3.1 The tight-binding approximation

Because of the small size of the device of only 1300 atoms, an atomistic grid is used, with one graphene atom at each site. The total wavefunction $\Psi(\mathbf{r})$ can then be expressed as a superposition of localized atomic p_z orbitals $\phi_{i,j}$, one at each atom (see section 2). The orbitals are numbered $i = 0, 1, N-1$ in the longitudinal and $j = 0, 1, M-1$ in the circumferential direction. In the basis of these orbitals, the Hamiltonian $\hat{H}$ becomes the $(N \cdot M) \times (N \cdot M)$ matrix H'. The interaction between different orbitals is assumed to be limited to the neighboring sites, which are connected by what is called a 'hopping matrix element' t (or also: 'overlap integral'). This approximation of tightly-bound electrons is also known as the *tight-binding approximation.* For this structure, the parameter t has the value $t = 3$ eV[6].

3.2 Bloch orbitals

Bloch's theorem states that the eigenstates $\psi(\mathbf{r})$ of an electron in a periodic lattice can be written in the form

$$\psi(\mathbf{r}) = e^{i\mathbf{k}\cdot\mathbf{r}}u(\mathbf{r}) \tag{5}$$

with $\mathbf{k}$ the wavevector inside the lattice and $u(\mathbf{r})$ a function with the same periodicity as the lattice. The $\psi(\mathbf{r})$ are then called the *Bloch states.* For graphene, each atom has 3 neighbours, making the Hamiltonian matrix H' in the basis of the $N \times M$ p_z orbitals $\phi_{i,j}(\mathbf{r})$ block-tridiagonal. Applying Bloch's theorem in the circumferential dimension, these orbitals are transformed into $N \times M$ Bloch orbitals $\chi_{n,q}$[1] by

$$\chi_{n,q}(\mathbf{r}) = \frac{1}{\sqrt{M}}\sum_{m=0}^{M-1} e^{iqR_m}\phi_{n,m}(\mathbf{r}), q = 0, 1, ..., M-1; R_m = \frac{2\pi m}{M}; n = 0, 1, .., N-1. \tag{6}$$

The Hamiltonian in terms of this basis is the tridiagonal matrix H, which can be uncoupled into M separate $N \times N$ tridiagonal Hamiltonian matrices $H_q, q = 0, 1, ..., M-1$. In Appendix A a more formal description is given of this transformation. The uncoupling of the two-dimensional problem into M one-dimensional problems is equivalent to treating each of the M distinct subbands in the band structure of the CN, each with a different wavenumber $k_q = (2\pi q)/(Ma)$, individually. This is visualised in figure 6.

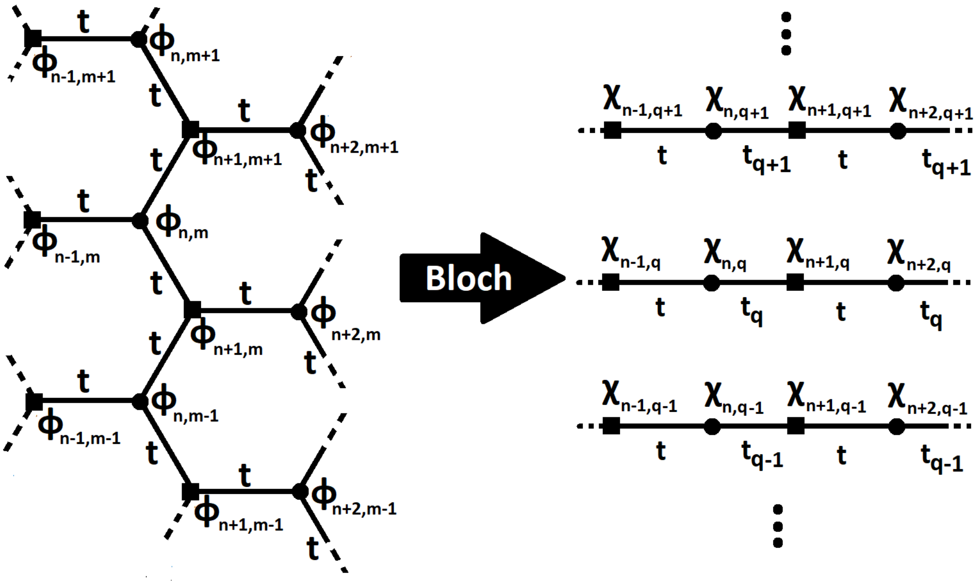

FIGURE 6: Visualisation of the transformation of the p_z orbitals $\phi_{n,m}$ orbitals into Bloch orbitals $\chi_{n,q}$ in the graphene lattice, and the corresponding decoupling of the problem.

Each of the N eigenstates $\psi_{n,q}$ of the Hamiltonian matrix H_q is then a linear combination of its N Bloch orbitals:

$$\psi_{n,q}(\mathbf{r}) = \sum_{j=0}^{N-1} c_{j,n,q}\chi_{j,q}(\mathbf{r}) \tag{7}$$

and the problem of solving the tight-binding Hamiltonian becomes the matrix-vector eigenvalue problem

$$\underline{H}_q \underline{c}_{n,q} = E_q \underline{c}_{n,q},$$

Following from the derivations in Appendix A, the interaction of $\chi_{j,q}$ in ring A with $\chi_{j-1,q}$ in the previous ring B is given by t and with $\chi_{j+1,q}$ in the following ring B by $t_q = 2t\cos\pi q/M$. This results in the following Hamiltonian matrix H_q:

$$\underline{H}_q = \begin{bmatrix} U_1 & t_q & & & & \\ t_q & U_2 & t & & & \\ & t & U_3 & t_q & & \\ & & \ddots & \ddots & \ddots & \\ & & & t & U_{N-1} & t_q \\ & & & & t_q & U_N \end{bmatrix}. \tag{8}$$

The $E_q(k)$ relation for the Hamiltonian matrix H_q is [6]

$$E_q(k)^{\pm} = \pm\sqrt{t^2 + t_q^2 + 2tt_q\cos(3ka/2)}. \tag{9}$$

The bandgap following from this band structure is

$$\begin{aligned}E_{g,q} &= E_q(0)^+ - E_q(0)^- = 2\sqrt{t^2 + t_q^2 + 2tt_q\cos(0)}\\ &= 2\sqrt{t^2 + 2^2t^2\cos^2(\pi q/M) + 2tt2\cos\pi q/M}\\ &= 2|t|\sqrt{1 + (2\cos(\pi q/M))^2 + 4\cos(\pi q/M)}\\ &= 2t\sqrt{(2\cos(\pi q/M) + 1)^2}\\ &= 2t|1 + 2\cos(\pi q/M)|. \end{aligned} \tag{10}$$

Figure 7 shows a plot of this band structure for $-\pi/a \leq k \leq \pi/a$, $q = 9$.

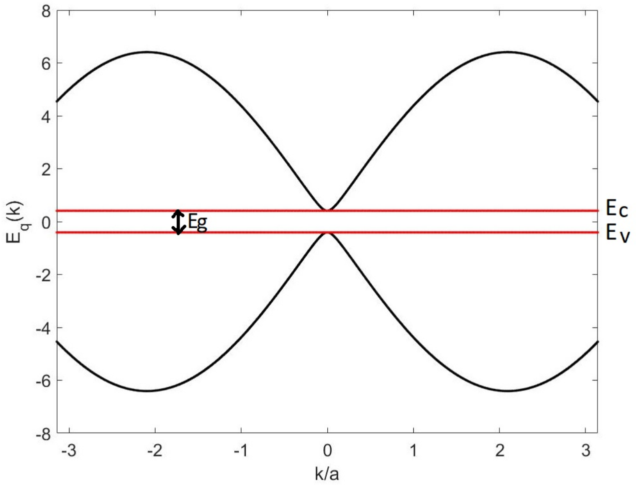

FIGURE 7: Band structure of carbon nanotube for subband $q = 9$, having a bandgap of $E_g = 0.82$ eV.

Subband $q = 9$ (or, equivalently: $q = 4$) has its band edges the closest to 0 eV. This means that increasing the voltage difference from 0 eV, $q = 9$ will be the first subband which lies inside the relevant energy range of the charge density and the current. Therefore, in the rest of the paper, only subband $q = 9$ will be considered and finally be modelled.

4 The Non-Equilibrium Green's Function Method

In section 3, the Hamiltonian matrices $H_1, ..., H_{13}$ for a (13,0) CN of length N are defined. Since only subband $q = 9$ will be modelled, only the matrix H_9 is used, and its notation is simplified to H in this section. The final model will deal with electron waves moving from one contact of the device to the other. This means that the problem which will be solved in the model is a slight modification of equation 4:

$$[EI - H]\Psi = S, \tag{11}$$

where E is a real number, I is the identity matrix and S is an excitation term due to a wave incident from one of the ends of the CN. The *Green's function*[2] for this problem is given by

$$G = [EI - H]^{-1}, \tag{12}$$

which is the response of the system to an impulse excitation inside the device. Finding the Green's function, i.e. calculating the inverse of $[EI - H]$, is equivalent to solving equation 11, since the solution Ψ can then be expressed in terms of G. This aspect will become visible in the fairly straightforward equations later in this section which use the Green's function to calculate the desired physical properties of the device.

4.1 Motivation behind the Green's function

The transformation of the problem from equation 11 to equation 12 may seem subtle and maybe even unnecessary. Therefore, a motivation has to be given to introduce the Green's function. The difficulty in solving the response of the system to the conatacts lies in the boundary conditions. In section 3, the Hamiltonian matrix was calculated by essentially assuming closed boundary conditions. This is inaccurate, since the nanotube is assumed to be infinite like in figure 4. Such a problem could be solved using periodic boundary conditions, but this does not suffice yet. In this model, there is a voltage difference between the two semi-infinite ends (the yellow parts of figure 4). This means that we have a non-equilibrium problem and need open boundary conditions [3]. For this infinitely long carbon nanotube actually an infinite-dimensional Hamiltonian matrix has to be solved. This is of course infeasible in the ordinary way, but fortunately the Green's function formalism provides a technique for solving this problem. The effects of the biased semi-inifinite ends can be "folded" into the device by adding two so-called *self-energy* terms to the finite $N \times N$ Hamiltonian matrix of the device.

4.2 The self-energies

The self-energies at the source and drain for this CN are two matrices of dimensions $N \times N$:

$$\Sigma_s(E) = \begin{bmatrix} t^2 g_s(E) & 0 & \dots & 0 \\ 0 & 0 & & \\ \vdots & & \ddots & \\ 0 & & & 0 \end{bmatrix} = \begin{bmatrix} t^2 g_s(E) & \\ & \end{bmatrix} \text{ (in simplified notation)} \tag{13}$$

and

$$\Sigma_d(E) = \begin{bmatrix} & \\ & t^2 g_d(E) \end{bmatrix}, \tag{14}$$

respectively, where the *surface Green's functions* $g_{s(d)}$ at the interface between the device and the left and right ends are given by

$$g_{s(d)}(E) = \frac{1}{2t^2(E-U_{s(d)})}\Big[-(E-U_{s(d)})^2 - t^2 + t_q^2 \pm \sqrt{\Big((E-U_{s(d)})^2 + t^2 - t_q^2\Big)^2 - 4t^2(E-U_{s(d)})^2}\Big]. \tag{15}$$

The derivations of equations 13, 14 and 15 are given in Appendix B.

Now that open boundary conditions have been implemented into the Green's function, one point is left to mention. The Green's function in matrix form is now

$$G(E) = \Big[EI - H - \Sigma_s(E) - \Sigma_d(E)]^{-1}, \tag{16}$$

but for this equation actually still two solutions are possible, which are called the retarded and advanced Green's functions G^R and G^A. These retarded and advanced solutions belong to two different types of open boundary conditions: either of outgoing waves that originate at the point of excitation or of incoming waves that dissapear at the point of excitation. In the context of this problem, only the retarded solution is relevant. To resolve this, an infinitesimal positive imaginary part $i\eta$ is added to the energy, resulting in the equation

$$G(E) = \Big[(E+i\eta)I - H - \Sigma_s(E) - \Sigma_d(E)]^{-1}, \tag{17}$$

for which the advanced Green's function becomes unbounded and therefore only the retarded Green's function is a solution.[2] From here on, the retarded Green's function will be referred to as simply the "Green's function" G, but note that later also $G^A = (G^R)^\dagger$ will be needed to calculate certain properties.

The final Green's function matrix used in the model is

$$G(E) = \tag{18}$$
$$\begin{bmatrix} (E+i\eta) - U_1 - t^2 g_s(E) & -t_q & & & \\ -t_q & (E+i\eta) - U_2 & -t & & \\ & \ddots & \ddots & \ddots & \\ & & & -t_q & (E+i\eta) - U_N - t^2 g_d(E) \end{bmatrix}^{-1}.$$

4.3 Results from the Green's function formalism

From the Green's function $G(E)$ and the self-energies $\Sigma_s(E)$ and $\Sigma_d(E)$, a couple of useful properties can be calculated. Their expressions are given here without derivations. All of them involve an integration over a range of energies, which is why the Green's function and the self-energies are given as functions of energy. For the theoretical background and physical interpretation of the expressions in the rest of the section, see [2].

The first property is called the *level broadening* and is defined as

$$\Gamma_{s(d)} = \Gamma_{s(d)} = i\Big(\Sigma_{s(d)} - \Sigma^\dagger_{s(d)}\Big). \tag{19}$$

The local density of states (LDOS) distributions D_s and D_d due to the left and the right contact, respectively, can be calculated from $G(E)$ and $\Gamma_{s(d)}(E)$ with the formula

$$D_{s(d)}(x,E) = D_{s(d)} = G\Gamma_{s(d)}G^\dagger. \tag{20}$$

These are probability density functions representing the amount of states which can be occupied by electrons at each energy. For an intrinsic (undoped), unbiased ($V_s = V_g = V_d = 0$) (13,0) CN with 100 rings, plots of the total LDOS

$$D(x, E) = D_s(x, E) + D_d(x, E) \tag{21}$$

and the spatially averaged density of states (DOS)

$$D_E(E) = \frac{1}{N} \sum_x D(x, E) \tag{22}$$

of all 13 subbands are given in figure 8.

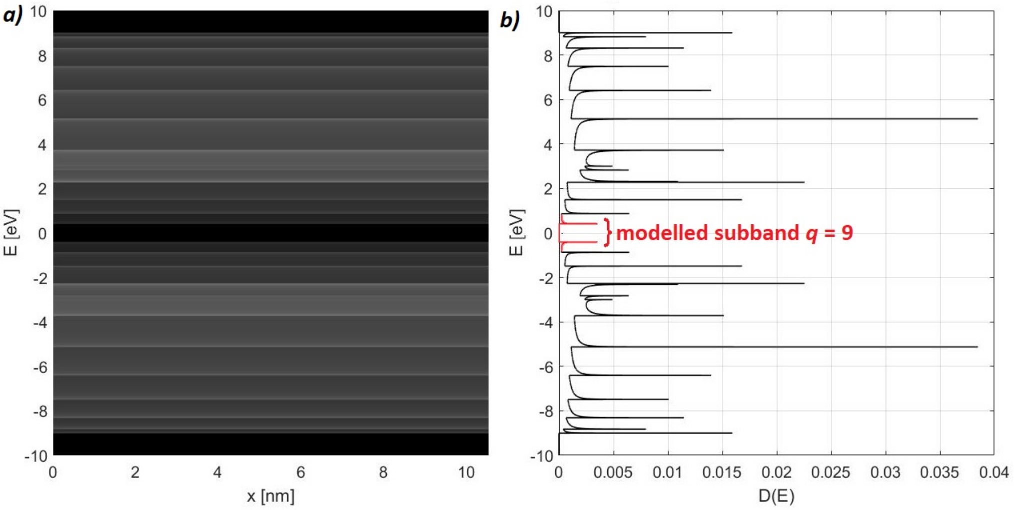

FIGURE 8: Plots for all 13 subbands of an intrinsic $(13, 0)$ CN of *a)* the LDOS $D(x, E)$, a higher brightness represents a higher LDOS, the distribution is plotted with a lower constract to improve visibility; *b)* the DOS $D_E(E)$.

The valence and conduction bands of the 13 subbands are clearly visible in b) and their positions are consistent with equation 9.
Another variable is the transmission $T(E)$, calculated by

$$T = \mathrm{Trace}(\Gamma_s G \Gamma_d G^\dagger). \tag{23}$$

The transmission $T(E)$ represents in this case the amount of channels at energy E through which electrons can move from one contact to the other. Figures 9a) and b) show the calculated $D(E)$ and $T(E)$ for subband $q = 9$ for configurations similar to figure 5d) and e), respectively.

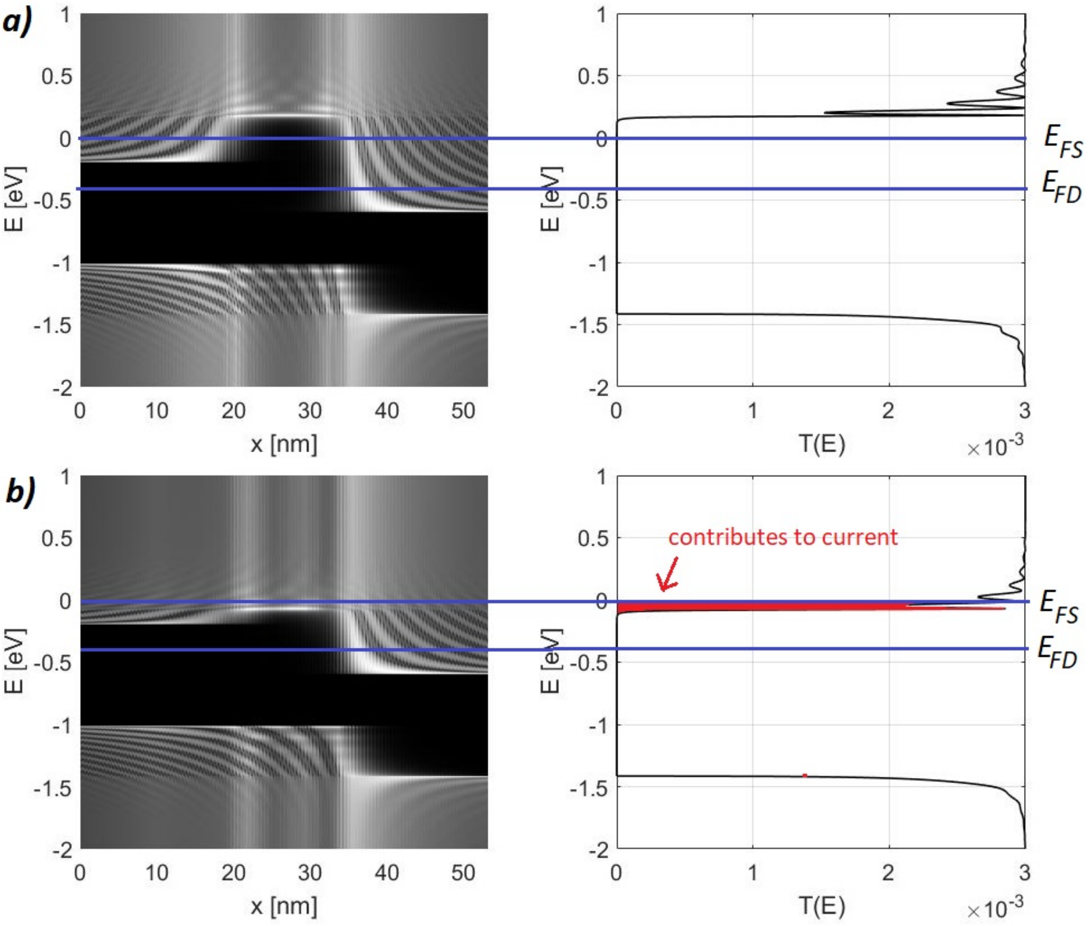

FIGURE 9: The LDOS $D(x, E)$ and the transmission $T(E)$ for subband $q = 9$ for *a)* $V_g = 0.25$V, *b)* $V_g = 0.5$V. Other parameters: $V_s = 0, V_d = 0.4, E_d = 0.61, N = 500, N_x = 175, M = 13, N_E = 1000$.

The two bright band edges contain the highest DOS. The pattern of curved white stripes is a result of both reflected and transmissed waves coming from both the source and drain contact. Inside the band gap, the transmission is 0. In a) it becomes visible from the transmission that even though a bias is applied to the device, no current will flow, since the energy window falls within the bandgap of the channel. When V_g is large enough, the transmission between the two Fermi levels becomes nonzero like in b) and a current can flow between the contacts. In the region $0.4 \leq V_g \leq 0.45$ this increase is expected to be exponential because of the exponential growth of the transmission here. This is also called the *subthreshold region*. After the transmission is maximal in the whole energy regime, the current is expected to be saturated and not increase further (for this subband).

4.3.1 Charge density

To start, it is good to note that charge neutrality holds for a CN without voltage differences. When considering only n-type doping, this means that

$$Q_{tot} = Q_v + Q_c + Q_a + Q_n = 0, \tag{24}$$

where Q_v is the total charge of electrons in the valence band, Q_c the total charge of electrons in the conduction band, Q_a the total charge of the positive carbon atom nuclei and Q_n the total charge of the positive ionized donor atoms. To show that the DOS calculated with the Green's function method is valid, Q_v is calculated for the device configuration of figure 8. This charge is expected to be

$$Q_e = (-e) \cdot N_{atoms} = (-e)13 \cdot 100 = (-e)1300, \tag{25}$$

with each graphene atom delivering one electron to the total electron pool ($e = 1.602 \cdot 10^{-19}$ C). This value can be verified by filling up the DOS contributions of the source and the drain, $D_s(E,x)$ and $D_d(E,x)$, up to the middle gap energy:

$$\begin{aligned} Q_v &= \sum_x Q_{v,s}(x) + Q_{v,d}(x) \\ &= \sum_x (-e)2\Big(\int_{-\infty}^{0} D_s(E,x)dE + \int_{-\infty}^{0} D_d(E,x)dE\Big), \end{aligned} \tag{26}$$

where the extra factor 2 is added to account for the 1/2-spin degeneracy of electrons. In this case, we can set the lower limit to -10 eV. For an energy step of $dE = 0.002$ eV, the integral is equal to $Q_v = 1300.5 \approx 1300$, as expected.
Now assuming a uniformly doped CN and still keeping the voltage zero everywhere, it is safe to say that $Q_v = -Q_a$, which implies that $Q_c = -Q_d$. Since Q_d is equal to e times the total number of donor atoms N_d, the following equality holds:

$$\begin{aligned} N_d = -\frac{1}{e}Q_c &= -\frac{1}{e}\sum_x Q_s(x) + Q_d(x) \\ &= \sum_x 2\Big(\int_{0}^{E_d} D_s(E,x)dE + \int_{0}^{E_d} D_d(E,x)dE\Big) \end{aligned} \tag{27}$$

where E_d is the Fermi level shift because of the doping as shown in figure 5a) of section 2. The energy difference E_d will be a parameter for the model and the doping concentration n_d in the source and drain contacts belonging to this E_d will be determined by calculating the integral in equation 27. The doping charge density $Q_n(x)$ is then calculated as

$$Q_n(x) = \begin{cases} eN_d/(2N_xM) & 0 \leq x \leq Nx \text{ or } N - N_x \leq x \leq N \\ 0 & \text{otherwise} \end{cases} \tag{28}$$

and is used in solving the Poisson's equation in section 5. A typical configuration of the device is shown in figure 5e), with applied gate and drain voltages (relative to the source voltage). The charge Q_c is calculated with the formula

$$Q_c(x) = (-e)2\Big(\int_{U(x)}^{E_{FS}} D_s(E,x)dE + \int_{U(x)}^{E_{FD}} D_d(E,x)dE\Big), \tag{29}$$

where E_{FS} and E_{FD} are the Fermi levels at the source and drain contacts, respectively. This charge is also used in solving the Poisson's equation.

4.3.2 Current

The current can be calculated with the *Landauer formula* using the transmission defined above:

$$I = \frac{4e}{h}\int_{E_{FD}}^{E_{FS}} T(E)dE \tag{30}$$

where h is the Planck constant

$$h = 4.135 \cdot 10^{-15} \text{ eV/s}.$$

This formula integrates over the relevant energy range to find the total amount of channels through which electrons can flow. One factor two is added because of the spin degeneracy of electrons (i.e. a total of 2 electrons can “use” the same channel) and another factor two because of “the valley degeneracy in the carbon nanotube energy band structure”[6]. This is a dimensionless number which is then multiplied with the current $I_0 = e/h$ of one moving electron.

5 The Poisson Equation

In the previous section the Green's function matrix was derived in equation 18. Using the Green's function formalism the charge density inside the device can be found. In this section, the charge density is used as the input for calculating the electrostatic potential distribution, which is again used in 12. The relation between the charge density and the potential is called the Poisson equation, which in differential form is given by

$$\nabla^2 \phi = -\frac{\rho}{\epsilon} \tag{31}$$

where ϕ is the potential (not to be confused with the p_z orbitals $\phi(\mathbf{r})$ from section 3), ρ the charge density and ϵ the permittivity of the medium.
The geometry of this device demands a Poisson solver in cylindrical coordinates. The Laplacian in cylindrical coordinates is given by[5]

$$\nabla^2 \phi = \frac{1}{r}\frac{\partial}{\partial r}\left(r\frac{\partial \phi}{\partial r}\right) + \frac{1}{r^2}\frac{\partial^2 \phi}{\partial \theta^2} + \frac{\partial^2 \phi}{\partial x^2}. \tag{32}$$

Defining the coordinate system like in figure 4 of section 2, it is assumed that

$$\frac{\partial^2 \phi}{\partial \theta^2} = 0. \tag{33}$$

Therefore, the Poisson problem becomes two-dimensional and is illustrated in figure 10.

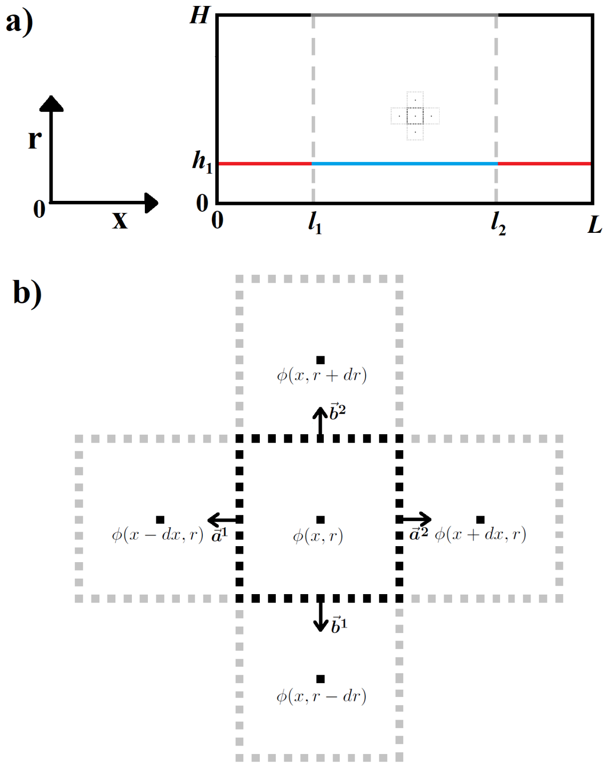

FIGURE 10: *a)* The carbon nanotube transistor in a two-dimensional coordinate system. The line at $0 \leq x \leq L, r = h_1$ represents the nanotube source, drain and channel surface; the line at $l_1 \leq x \leq l_2, r =\leq H$ represents the gate. *b)* The five-point stencil used for solving the Poisson equation.

In section 4 the charge density $Q(x)$ is calculated, which is actually the point charge of each ring of the CN. After a two-dimensional grid is defined on figure 10a), $Q(x)$ are used as input for the charge densities inside the grid cells at $h_1 = r = 0.51$ nm, while the charge density inside other grid cells is set to zero. For this problem the following boundary conditions (B.C.'s) are defined for $\phi(x,r)$ and its partial derivatives. At all four boundaries Neumann B.C.'s are chosen:

$$\begin{cases} \left.\frac{\partial\phi}{\partial x}\right|_{(0,r)} = \left.\frac{\partial\phi}{\partial x}\right|_{(L,r)} = 0 & \text{for } 0 \le r \le H, \\ \left.\frac{\partial\phi}{\partial r}\right|_{(x,0)} = \left.\frac{\partial\phi}{\partial r}\right|_{(x,H)} = 0 & \text{for } 0 \le x \le L. \end{cases} \tag{34}$$

Furthermore, at the source, gate and drain boundaries extra Dirichlet B.C.'s are chosen:

$$\begin{cases} \phi(0,h_1) = U_s, \\ \phi(L,h_1) = U_d, \\ \phi(x,H) = U_g \quad \text{for } l_1 \le x \le l_2. \end{cases} \tag{35}$$

The Poisson equation 31 can be written in integral form using Gauss's law, which relates the flux of the electric field (in this case the D-field) through a closed surface to the total charge enclosed by the surface. This gives

$$\oiint_S \vec{\mathbf{D}} \cdot \mathrm{d}\vec{\boldsymbol{a}} = Q_{\text{free}}, \tag{36}$$

where

$$\vec{\mathbf{D}}(x,r) = \epsilon\vec{\mathbf{E}}(x,r) \tag{37}$$

and

$$\vec{\mathbf{E}}(x,r) = -\left|\nabla\phi\right._{(x,r)} = -\left.\frac{\partial\phi}{\partial x}\right|_{(x,r)}\hat{\mathbf{x}} - \left.\frac{\partial\phi}{\partial r}\right|_{(x,r)}\hat{\mathbf{r}}. \tag{38}$$

For the volume element around (x,r) drawn in figure 10b), the surface S consists of four surface areas, a^1, a^2, b^1 and b^2. By dividing figure 10 into a two-dimensional grid and discretising the derivatives of equation 38, the problem with its boundary conditions can be turned into an equation of the form

$$Ax = b$$

, where A is a five-diagonal matrix and x and b contain the potential and charge density at all the grid cells, respectively. The derivation of matrix A, which also uses the finite-difference method, can be found in Appendix C. The potential at the nanotube surface for a given charge distribution is obtained by solving

$$x = A\backslash b \tag{39}$$

with the MATLAB "backslash" operator \.

6 Results

The final program combines the results from section 3, 4 and 5, as shown before in figure 1.

6.1 Self-consistency

In the iterative calculation, the potential and charge distributions $U(x)$ and $Q(x)$ (more precisely, $Q_c(x)$) are updated each iteration i. The deviations ΔU_i and ΔQ_i at iteration i are defined as

$$\Delta U_i = \sum_x |U_i(x) - U_{i-1}(x)|, \tag{40}$$

$$\Delta Q_i = \sum_x |Q_i(x) - Q_{i-1}(x)|. \tag{41}$$

When both $\Delta U, \Delta Q < \delta = 10^{-4}$, the solution is said to have converged and the current is calculated. For the parameters

$$V_s = 0\text{V}, V_d = 0.25\text{V}, E_d = 0.61\text{eV}, q = 9, N = 100, N_x = 40, M = 13, N_E = 500, \tag{42}$$

the solution converges within 7 iterations, as shown in figure 11.

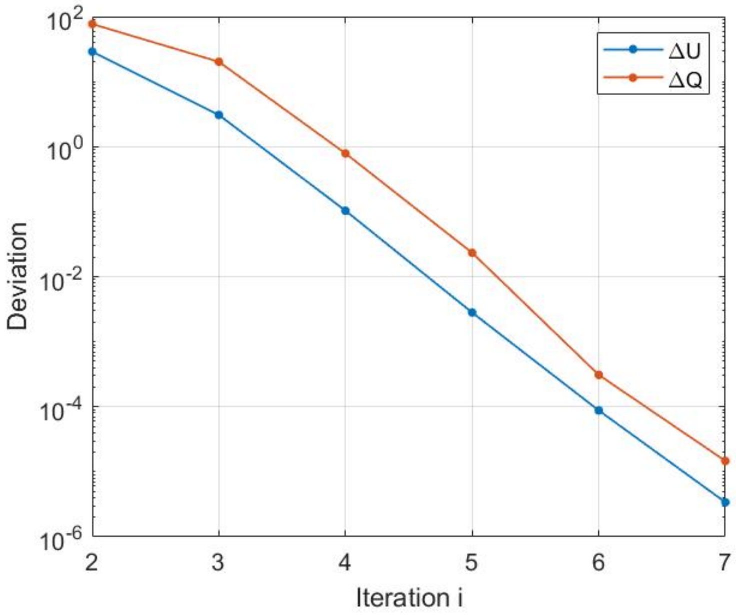

Figure 11: Convergence of self-consistent calculation for the parameters of equation 42.

The potential and charge distributions for the first and last iteration are given in figure 12.

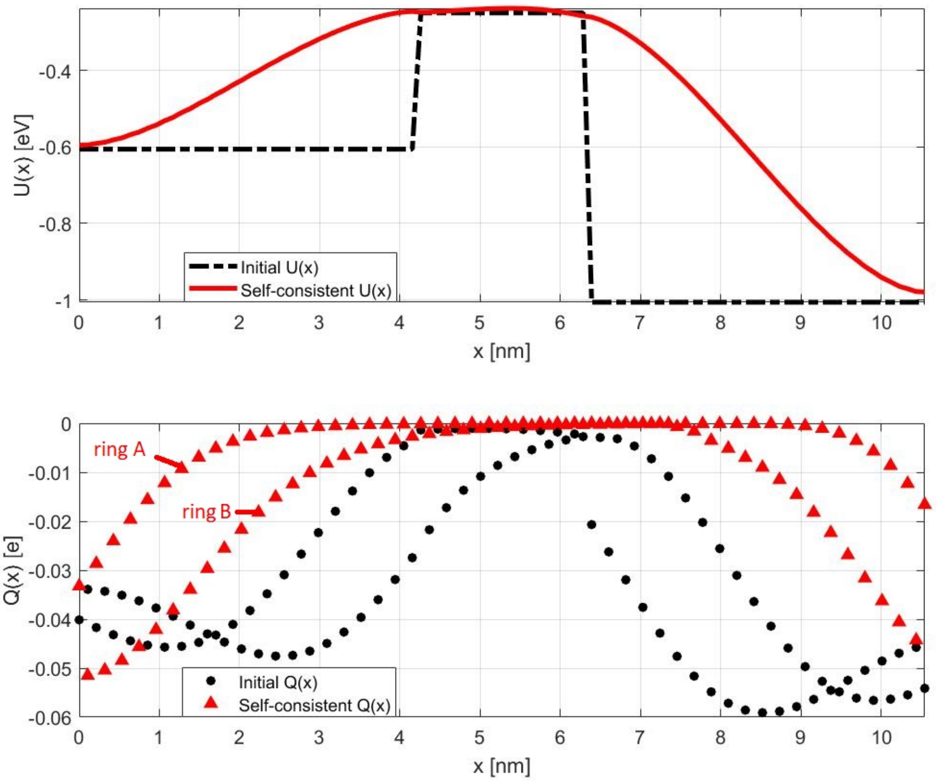

FIGURE 12: Solution at first and last iteration for the parameters of equation 42, for *a)* $U(x)$ and *b)* $Q(x)$.

Visible is that the potential becomes continuous when self-consistency is reached. What is also remarkable is that the charge distribution oscillates heavily throughout the device, but is continuous when considering only one of the two rings, A or B.

6.2 Performance transistor

The central characteristic of a MOSFET is its ability to alter the current I_{sd} going from source to drain several orders of magnitude by applying a relatively small voltage to the gate. The slope of "switching" the transistor "on" and "off" is called the "subthreshold slope". Figure 13 shows this exponential increase of the current in the subthreshold region for the CNT, displaying a similar curve as in [6], figure 9. The maximal slope in the subthreshold region is called the subthreshold swing (SS) and can be calculated as

$$SS = \Delta V_g / \Delta \log_{10}(I_{sd}). \tag{43}$$

For the curve in figure 13 $SS = 111$ mV/dec, which is comparable to the values found in [10]. Beyond this slope, further increasing V_g has a increasingly smaller effect on the current until the current becomes constant.

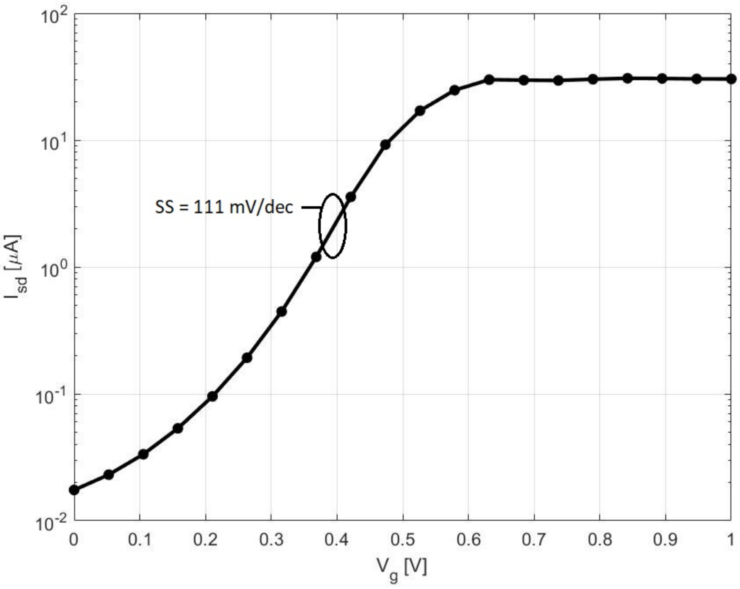

FIGURE 13: $I_{sd} - V_g$ characteristics for $V_s = 0\text{V}, V_d = 0.4\text{V}, E_d = 0.61\text{eV}, q = 9, N = 100, N_x = 40, M = 13, N_E = 100$.

Another result is the current behaviour in the "on" regime in figure 14, showing similar graphs as in figure 4 of [7]. Also this result confirms the validity of the transport calculation of the program.

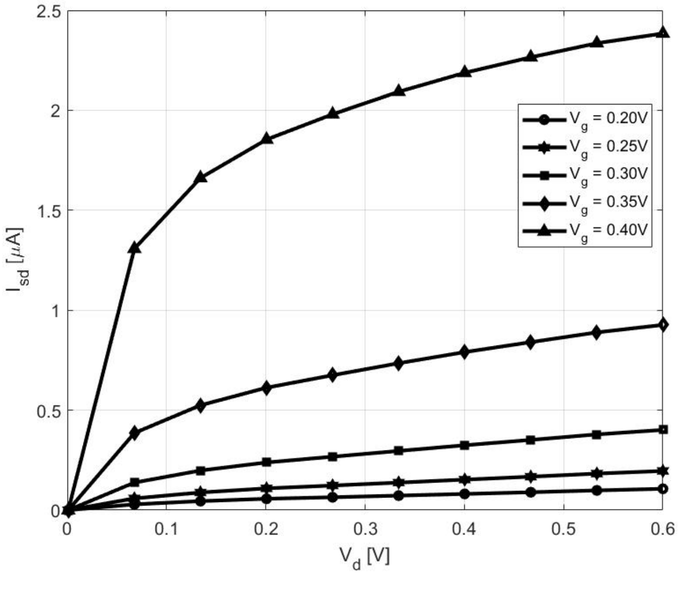

FIGURE 14: $I_{sd} - V_d$ characteristics for varying V_g, $V_s = 0\text{V}, E_d = 0.61\text{eV}, q = 9, N = 100, N_x = 40, M = 13, N_E = 100$.

7 Discussion

The results in section 6 are promising. The fast convergence in figure 11 confirms the validity of this method to obtain self-consistency for the Schrödinger equation and the Poisson equation in this non-equilibrium problem. The result in figure 13 gives the characteristic I-V curve of the device which confirms the expectations set by figure 5. The subthreshold slope appears at $V_g = 0.4\text{V}$ and the current becomes saturated at around $V_g = 0.7\text{V}$, as predicted by the explanation given to figure 9. Nevertheless, there are still some points which need further attention in order to improve the model.

First of all, it was not straightforward to implement the n-type doping of the source and drain into the model. As a work-around, the amount of extra electron charge in the device as a result of raising the Fermi level by a specific amount Ed was calculated in order to find the respective donor concentration n_d. It is expected that from solid-state physics theory an analytic expression for $n_d(Ed)$ can be found and used in the model.

Furthermore, the inverse calculation in finding the Green's function by using the built-in inv() MATLAB function is computationally intensive. A more efficient method could be found using Gaussian elimination, as already mentioned in [6].

Finally, to make the model more complete, scattering effects sholud be added to the model. In this model ballistic transport is assumed, which means that the mean free path of electrons is assumed to be much longer than the length of the nanotube. For the scale of this device, the ballistic limit is already a good approximation, but phonon scattering effects should be incorporated to further improve the accuracy of the model. The non-equilibrium's Green's function (NEGF) method already provides a basis for this: an extra self-energy term Σ_{scat} can be added to the ballistic model like explained in [7]. This was another motivation for using the NEGF method for this model.

The aim of this paper was to give a detailed description of the building process of a CNT model. Looking forward, this model could be used to test different versions of the carbon nanotube to find the optimal configuration. Examples of parameters that could be investigated are the gate length, the channel length, the distance between gate and channel and the doping concentrations of the contacts as well as the channel.

8 Appendices

Appendix A: Derivation of the Hamiltonian matrices in the Bloch orbital basis

To start, let

$$\mathcal{H} = L^2(\mathbb{R}^3) \tag{44}$$

be the *complex Hilbert space* consisting of the set of all square-integrable functions

$$f : \mathbb{R}^3 \to \mathbb{C}, \qquad \int f^*(\mathbf{r}) f(\mathbf{r}) d\mathbf{r} = 1 \tag{45}$$

together with the *inner product* $\langle \cdot | \cdot \rangle$ defined by

$$\langle \phi | \psi \rangle = \int \phi(\mathbf{r})^* \psi(\mathbf{r}) d\mathbf{r}. \tag{46}$$

Following the bra-ket notation, the set of p_z orbitals

$$S = \Big\{ |\phi_{i,j}\rangle \in \mathcal{H} : i = 0, 1, ..., N-1, j = 0, 1, ..., M-1 \Big\}$$

of the $N \times M$ carbon nanotube lattice is an *orthonormal set* of $\mathcal{H}$, i.e.

$$\left\langle \phi_{i',j'} \middle| \phi_{i,j} \right\rangle = \delta_{ii'} \delta_{jj'} \qquad \forall \left| \phi_{i,j} \right\rangle, \left| \phi_{i',j'} \right\rangle \in S, \tag{47}$$

and is therefore also linearly independent. For each $|\phi_{i,j}\rangle \in S$, define the *neighbor set*

$$N(|\phi_{i,j}\rangle) \subseteq S \tag{48}$$

as the set of all vectors in S "adjacent" to $|\phi_{i,j}\rangle$ in the lattice which is partly given in figure 6. Following from the tight-binding approximation, the (Hermitian) *Hamiltonian operator* $\hat{H}$ on S is defined as

$$\begin{gathered} \hat{H} : S \to H, \\ \left\langle \phi_{i',j'} \middle| \hat{H} \phi_{i,j} \right\rangle = \begin{cases} U_i & \left| \phi_{i',j'} \right\rangle = \left| \phi_{i,j} \right\rangle, \\ t & \left| \phi_{i',j'} \right\rangle \in N(|\phi_{i,j}\rangle), \\ 0 & \text{otherwise.} \end{cases} \end{gathered} \tag{49}$$

A linear combination of vectors in S

$$|\psi\rangle = \sum_{i=0}^{N-1} \sum_{j=0}^{M-1} c_{,i,j} \left| \phi_{i,j} \right\rangle \in \mathcal{H} \tag{50}$$

is said to be an *eigenstate of* $\hat{H}$ if it holds that

$$\exists E \in \mathbb{R} : \hat{H} |\psi\rangle = E |\psi\rangle. \tag{51}$$

The real number E is then called the *eigenenergy* of $|\psi\rangle$.
In $\mathcal{H}$ the so-called *Bloch orbitals* $|\chi_{j,k}\rangle$[1] are defined as

$$|\chi_{j,k}\rangle = \frac{1}{\sqrt{M}} \sum_{m=0}^{M-1} e^{ikR_m} |\phi_{j,m}\rangle \in \mathcal{H}, \qquad j = 0, 1, ..., N-1, k = 0, 1, ..., M-1, R_m = \frac{2\pi m}{M}.$$

$$(52)$$

For all $\left|\chi_{j',k'}\right\rangle, \left|\chi_{j,k}\right\rangle \in \mathcal{H}$ it holds that

$$\begin{aligned}
\left\langle \chi_{j',k'} \middle| \chi_{j,k} \right\rangle &= \Big(\frac{1}{\sqrt{M}} \sum_{m=0}^{M-1} e^{-ik'R_m} \left\langle \phi_{j',m} \right| \Big) \Big(\frac{1}{\sqrt{M}} \sum_{N=0}^{M-1} e^{ikR_n} \left| \phi_{j,n} \right\rangle \Big) \\
&= \frac{1}{M} \sum_{m=0}^{M-1} e^{-ik'R_m} \left\langle \phi_{j',m} \right| \Big(\sum_{N=0}^{M-1} e^{ikR_n} \left| \phi_{j,n} \right\rangle \Big) \\
&= \frac{1}{M} \sum_{m=0}^{M-1} \sum_{N=0}^{M-1} e^{-ik'R_m} e^{ikR_n} \left\langle \phi_{j',m} \middle| \phi_{j,n} \right\rangle \\
&= \frac{1}{M} \sum_{m=0}^{M-1} \sum_{N=0}^{M-1} e^{-ik'R_m} e^{ikR_n} \delta_{j'j} \delta_{mn} \\
&= \frac{1}{M} \sum_{m=0}^{M-1} e^{-ik'R_m} e^{ikR_m} \delta_{j'j} \\
&= \frac{1}{M} \delta_{j'j} \sum_{m=0}^{M-1} e^{iR_m(k-k')} \\
&= \delta_{j'j} \delta_{k'k}.
\end{aligned} \tag{53}$$

Therefore, the set of Bloch orbitals is also orthonormal. After some other results, such as that

$$\left\langle \chi_{j',k'} \middle| \hat{H} \chi_{j,k} \right\rangle = 0 \qquad \text{for } k' \neq k, \tag{54}$$

it follows is that the eigenstates of $\hat{H}$ are of the form

$$\left|\psi_{n,q}\right\rangle = \sum_{j=0}^{N-1} c_{j,n,q} \left|\chi_{j,k}\right\rangle, \qquad n = 0, ..., N-1, q = 0, ..., M-1. \tag{55}$$

The problem of finding the coefficients $c_{j,n,q}$ can be written as a matrix-eigenvalue vector equation in the basis of the Bloch orbitals $\left|\chi_{0,q}\right\rangle, ..., \left|\chi_{N-1,q}\right\rangle$:

$$\hat{H} \left|\psi_{n,q}\right\rangle = E_{n,q} \left|\psi_{n,q}\right\rangle \rightarrow \underline{\underline{H}}_q \underline{c}_{n,q} = E_q \underline{c}_{n,q},$$

where

$$\underline{\underline{H}}_q = \begin{bmatrix} \left\langle \chi_{0,q} \middle| \hat{H}\chi_{0,q} \right\rangle & \left\langle \chi_{0,q} \middle| \hat{H}\chi_{1,q} \right\rangle & \cdots & \left\langle \chi_{0,q} \middle| \hat{H}\chi_{N-1,q} \right\rangle \\ \left\langle \chi_{1,q} \middle| \hat{H}\chi_{0,q} \right\rangle & \left\langle \chi_{1,q} \middle| \hat{H}\chi_{1,q} \right\rangle & \cdots & \left\langle \chi_{1,q} \middle| \hat{H}\chi_{N-1,q} \right\rangle \\ \vdots & \vdots & \ddots & \vdots \\ \left\langle \chi_{N-1,q} \middle| \hat{H}\chi_{0,q} \right\rangle & \left\langle \chi_{N-1,q} \middle| \hat{H}\chi_{1,q} \right\rangle & \cdots & \left\langle \chi_{N-1,q} \middle| \hat{H}\chi_{N-1,q} \right\rangle \end{bmatrix} \tag{56}$$

The coefficients of $\underline{\underline{H}}_q$ are derived in the following way. Fixing for example the state $\left|\chi_{n,q}\right\rangle$ of figure 6,

$$N(\left|\phi_{n,j}\right\rangle) = \Big\{ \left|\phi_{n-1,j}\right\rangle, \left|\phi_{n+1,j}\right\rangle, \left|\phi_{n+1,j+1}\right\rangle \Big\}, \qquad j = 0, ..., M-1. \tag{57}$$

Therefore,

$$\begin{aligned}
\hat{H}\left|\chi_{n,q}\right\rangle &= \frac{1}{\sqrt{M}}\sum_{m=0}^{M-1} e^{iqR_m}\hat{H}\left|\phi_{n,m}\right\rangle \\
&= \frac{1}{\sqrt{M}}\sum_{m=0}^{M-1} e^{iqR_m}\Big[t\left|\phi_{n-1,m}\right\rangle + t\left|\phi_{n+1,m}\right\rangle + t\left|\phi_{n+1,m+1}\right\rangle + U_n\left|\phi_{n,m}\right\rangle\Big] \\
&= t\left|\chi_{n-1,q}\right\rangle + t\left|\chi_{n+1,q}\right\rangle + t\Big(\sum_{m=0}^{M-1} e^{-iqR_1}e^{iqR_{m+1}}\left|\phi_{n+1,m+1}\right\rangle\Big) + U_n\left|\chi_{n,q}\right\rangle \\
&= t\left|\chi_{n-1,q}\right\rangle + t\Big(1+e^{-iqR_1}\Big)\left|\chi_{n+1,q}\right\rangle + U_n\left|\chi_{n,q}\right\rangle .
\end{aligned} \tag{58}$$

The exponential term can be rewritten as

$$\begin{aligned}
\Big\langle\chi_{n+1,q}\Big|\hat{H}\chi_{n,q}\Big\rangle &= t(1+e^{-iqR_1}) \\
&= te^{-iqR_1/2}\Big(e^{+iqR_1/2}+e^{-iqR_1/2}\Big) \\
&= e^{-iqR_1/2}2t\cos(qR_1/2).
\end{aligned} \tag{59}$$

For calculating the charge density and the current, the phase factor of equation 59 can be omitted[6], therefore it is convenient to define

$$t_q = 2t\cos(qR_1/2) = 2t\cos(\pi q/M). \tag{60}$$

The final expression of $\underline{H}_q$ is

$$\underline{H}_q = \begin{bmatrix} U_1 & t_q & & & & \\ t_q & U_2 & t & & & \\ & t & U_3 & t_q & & \\ & & \ddots & \ddots & \ddots & \\ & & & t & U_{N-1} & t_q \\ & & & & t_q & U_N \end{bmatrix}. \tag{61}$$

Appendix B: Derivation of the self-energy matrices

In this problem, an analytic expression can be found for the self-energy matrices Σ_s and Σ_d. To start, only the coupling of the device to the left infinite end is considered. The total Hamiltonian matrix of device and left end H_{tot} consists of the infinite-dimensional matrix H_s of the left end, the $N \times N$ matrix H of the device, and the coupling τ between the two. This is visualised in figure 15.

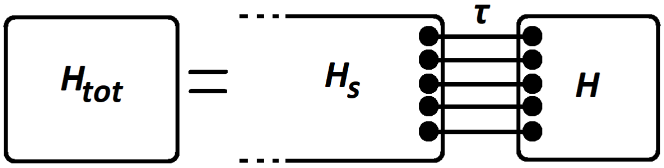

FIGURE 15: Visualisation of the coupling of the Hamiltonian matrix of the finite device to the left semi-infinite end.

In matrix form, this is given by

$$H_{tot} = \begin{bmatrix} H_s & -\tau \\ -\tau^\dagger & H \end{bmatrix}. \tag{62}$$

In this context, it is convenient to define for H_{tot}, H_s and H the auxillary matrices

$$A = (E + i\eta)I - H \tag{63}$$

resulting in the expression

$$A_{tot} = \begin{bmatrix} A_s & -\tau \\ -\tau^\dagger & A \end{bmatrix}. \tag{64}$$

Since the coupling between the left end and device equals the coupling of a ring B with the following ring A, the coupling matrices can already be identified as

$$\tau = \begin{bmatrix} & \\ t & \end{bmatrix}, \qquad \tau^\dagger = \begin{bmatrix} & t \\ & \end{bmatrix}. \tag{65}$$

Using equations 18 and 64 the total Green's function matrix G_{tot} can be rewritten as

$$G_{tot} = \begin{bmatrix} G_s & \bullet_1 \\ \bullet_2 & G \end{bmatrix} = \begin{bmatrix} A_s & -\tau \\ -\tau^\dagger & A \end{bmatrix}^{-1}, \tag{66}$$

where $\bullet_1$ and $\bullet_2$ are placeholders for parts of the Green's function matrix. From this matrix a system of equations can be extracted and solved for G:

$$\begin{cases} \bullet_2 A_s - G\tau^\dagger = 0, \\ -\bullet_2\,\tau + GA = I \end{cases} \Rightarrow \begin{cases} \bullet_2 = G\tau^\dagger A_s^{-1}, \\ -\bullet_2\,\tau + GA = I \end{cases} \quad \Rightarrow -G\tau^\dagger A_s^{-1}\tau + GA = I \Rightarrow$$
$$G = [A - \tau^\dagger A_s^{-1}\tau]^{-1}. \tag{67}$$

Defining

$$\Sigma_s = \tau^\dagger A_s^{-1}\tau \tag{68}$$

and numbering the diagonals of A_s^{-1} like

$$A_s^{-1} = \begin{bmatrix} \ddots & & \\ & g_2 & \\ & & g_1 \end{bmatrix}$$

results in

$$G = [A - \Sigma_s]^{-1} \tag{69}$$

and

$$\Sigma_s = \begin{bmatrix} & t \\ & \end{bmatrix} \begin{bmatrix} \ddots & & \\ & g_2 & \\ & & g_1 \end{bmatrix} \begin{bmatrix} & \\ t & \end{bmatrix} = \begin{bmatrix} t^2 g_1 & \\ & \end{bmatrix} = \begin{bmatrix} t^2 g_s & \\ & \end{bmatrix}. \tag{70}$$

Σ_s is called the *self-energy* at the source contact and g_s is called the *surface Green's function* for the first node inside the left end. The symmetry inside H_s is used to find an expression for g_s. The Green's function matrix G_s of the source can be divided up into the matrix part of the first ring of the left end g_1 and the rest of the left end G'_s:

$$\begin{bmatrix} G_{s'} & \bullet_3 \\ \bullet_4 & g_1 \end{bmatrix} = \begin{bmatrix} \ddots & & \\ & g_2 & \\ & & g_1 \end{bmatrix} = \begin{bmatrix} \ddots & \ddots & & & \\ \ddots & \ddots & -t_q & & \\ & -t_q & E-U_s & -t & \\ & & t & E-U_s & -t_q \\ & & & -t_q & E-U_s \end{bmatrix}^{-1} \tag{71}$$

.

The potential inside the left end has the constant value U_s. From this, the following identities can be extracted and an expression for g_s can be found:

$$\begin{cases} g_1 = [E - U_s - t_q g_2 t_q]^{-1}, \\ g_2 = [E - U_s - t g_3 t]^{-1}, \\ g_m = g_{m+2}, \qquad m = 0, 1, ... \end{cases} \Rightarrow$$

$$\begin{aligned} g_1 &= [E - U_s - t_q^2[E - U_2 - t^2 g_1]^{-1}]^{-1} \\ &= \frac{1}{E - U_s - t_q^2 \frac{1}{E - U_s - t^2 g_1}} \\ &= \frac{E - U_s - t^2 g_1}{(E - U_s)[E - U_s - t^2 g_1] - t_q^2} \Rightarrow \end{aligned}$$

$$\begin{aligned} &\Big((E - U_s)^2 - t_q^2\Big) g_1 - (E - U_s) t^2 g_1^2 = E - U_1 - t^2 g_1 \Rightarrow \\ &(E - U_s) t^2 g_1^2 + \Big(- t^2 + t_q^2 - (E - U_s)^2 \Big) g_1 + (E - U_s) = 0 \Rightarrow \end{aligned}$$

$$\begin{aligned} g_s = g_1 = \frac{1}{2t^2(E - U_s)} \Big[&- (E - U_s)^2 - t^2 + t_q^2 \\ &\pm \sqrt{\Big((E - U_s)^2 + t^2 - t_q^2\Big)^2 - 4t^2(E - U_s)^2} \Big]. \end{aligned} \tag{72}$$

The self-energy at the drain can be found in a similar way:

$$\Sigma_d = \begin{bmatrix} & \\ & t^2 g_d \end{bmatrix}, \tag{73}$$

where

$$\begin{aligned} g_d = \frac{1}{2t^2(E - U_d)} \Big[&- (E - U_d)^2 - t^2 + t_q^2 \\ &\pm \sqrt{\Big((E - U_d)^2 + t^2 - t_q^2\Big)^2 - 4t^2(E - U_d)^2} \Big]. \end{aligned} \tag{74}$$

8.1 Appendix C: Discretising the Poisson's problem

To discretise the Poisson's equation problem defined in section 5, the area of figure 10 is first divided into a two-dimensional grid:

$$\begin{aligned} &\phi(x_i, r_j) \to \phi_{i,j}, \\ &x_i = iL/(N-1), i = 0, ..., N-1, \\ &r_j = jK/(H-1), j = 0, ..., H-1, \end{aligned} \tag{75}$$

where N is the amount of rings of the CNT and K is a grid parameter set at 15. This implies that the grid cell length and height are given by

$$\begin{aligned}
&\mathrm{d}x \to \Delta x = L/(N-1) = \frac{3}{4}a,\\
&\mathrm{d}r \to \Delta r = H/(K-1).
\end{aligned} \tag{76}$$

The grid cell length Δx is equal to the average distance between two rings. The four surfaces of the grid cell around grid point $\phi_{i,j}$ are derived by considering the geometry in figure 4:

$$\begin{aligned}
a^1_{i,j} &= \pi\Big(r_j + \frac{\Delta r}{2}\Big)^2 - \pi\Big(r_j - \frac{\Delta r}{2}\Big)^2\\
&= \pi\Big(r_j^2 + r_j\Delta r + \frac{\Delta r^2}{4} - r_j^2 + r_j\Delta r - \frac{\Delta r^2}{4}\Big)\\
&= 2\pi r_j \Delta r, \qquad (77)\\
a^2_{i,j} &= a_1(x, r_j) = 2\pi r_j \Delta r,\\
b^1_{i,j} &= 2\pi\Big(r_j - \frac{\Delta r}{2}\Big)\Delta x \text{ and}\\
b^2_{i,j} &= 2\pi\Big(r_j + \frac{\Delta r}{2}\Big)\Delta x.
\end{aligned}$$

Furthermore, the finite-difference method discretises the partial derivative in the x-direction by

$$\frac{\partial \phi}{\partial x}\bigg|_{(x_i, r_j)} = \lim_{\mathrm{d}x \to 0} \frac{\phi(x_i + \mathrm{d}x\,, r_i) - \phi(x_i, r_i)}{\mathrm{d}x} \to \frac{\Delta\phi_{i,j}}{\Delta x} = \frac{\phi_{i+1,j} - \phi_{i,j}}{\Delta x} \tag{78}$$

and in the r-direction by

$$\frac{\partial \phi}{\partial r}\bigg|_{(x_i, r_j)} = \lim_{\mathrm{d}r \to 0} \frac{\phi(x_i, r_i + \mathrm{d}r) - \phi(x_i, r_i)}{\mathrm{d}r} \to \frac{\Delta\phi_{i,j}}{\Delta r} = \frac{\phi_{i,j+1} - \phi_{i,j}}{\Delta r}. \tag{79}$$

Therefore, for $i = 0, ..., N-1, j = 0, ..., K-1$:

$$\begin{aligned}
\frac{q_{i,j}}{\epsilon} =& \frac{a^1_{i,j}}{\Delta x}\Big(\phi_{i,j} - \phi_{i-1,j}\Big) + \frac{a^2_{i,j}}{\Delta x}\Big(\phi_{i,j} - \phi_{i+1,j}\Big) +\\
& \frac{b^1_{i,j}}{\Delta r}\Big(\phi_{i,j} - \phi_{i,j-1}\Big) + \frac{b^2_{i,j}}{\Delta r}\Big(\phi_{i,j} - \phi_{i,j+1}\Big) \Rightarrow
\end{aligned}$$

$$\begin{aligned}
\frac{q_{i,j}}{\epsilon} = \Big(\frac{a^1_{i,j}}{\Delta x} + \frac{a^2_{i,j}}{\Delta x} + \frac{b^1_{i,j}}{\Delta x} + \frac{b^2_{i,j}}{\Delta x}\Big)\phi_{i,j}&\\
-\frac{a^1_{i,j}}{\Delta x}\phi_{i-1,j} - \frac{a^2_{i,j}}{\Delta x}\phi_{i+1,j}&\\
-\frac{b^1_{i,j}}{\Delta x}\phi_{i,j-1} - \frac{b^2_{i,j}}{\Delta x}\phi_{i,j+1}&.
\end{aligned} \tag{80}$$

The Neumann B.C.'s of equation 34 can be incorporated by setting

$$\begin{aligned}
&a^1_{0,j} = a^2_{N-1,j} - 0 \qquad i = 0, ..., N-1\\
&b^1_{i,0} = b^2_{i,K-1} = 0 \qquad j = 0, ..., K-1.
\end{aligned} \tag{81}$$

The Dirichlet B.C.'s of equation 35 are taken as additional B.C.'s:

$$\begin{cases} \phi_{0,j} & = U_s \qquad \text{for } j \text{ s.t. } r_j = h_1, \\ \phi_{N-1,j} & = U_d \qquad \text{for } j \text{ s.t. } r_j = h_1, \\ \phi_{i,K-1} & = U_g \qquad \text{for } i \text{ s.t. } l_1 \leq x_i \leq l_2. \end{cases} \tag{82}$$

This is a linear system of equations which can be written in matrix form as

$$Ax = b, \tag{83}$$

where A is a five-diagonal matrix which has a few extra rows containing the Dirichlet B.C.'s, x is a column vector of length N representing the potentials $\phi_{i,j}$ at every grid point and b is a column vector representing the charge densities $q_{i,j}$ at every grid point together with the Dirichlet B.C. potentials. The charge densities $q_{i,j}$ are given by

$$q_{i,j} = \begin{cases} Q_c(x_i) + Q_n(x_i) & \text{for } j \text{ s.t. } r_j = h_1, \\ 0 & \text{otherwise.} \end{cases} \tag{84}$$

References

[1] Geert Brocks. Graphene: an introduction. Technical report, University of Twente, 2015.

[2] Supriyo Datta. *Electronic Transport in Mesoscopic Systems.* Cambridge University Press, sep 1995.

[3] Supriyo Datta. Nanoscale device modeling: the Green's function method. *Superlattices and Microstructures*, 28(4):253–278, oct 2000.

[4] Alexandra L. Gorkina, Alexey P. Tsapenko, Evgenia P. Gilshteyn, Tatiana S. Koltsova, Tatiana V. Larionova, Alexander Talyzin, Anton S. Anisimov, Ilya V. Anoshkin, Esko I. Kauppinen, Oleg V. Tolochko, and Albert G. Nasibulin. Transparent and conductive hybrid graphene/carbon nanotube films. *Carbon*, 100:501–507, apr 2016.

[5] David Jeffery Griffiths. *Introduction to Electrodynamics.* Pearson Education, Inc., fourth edition, 2013.

[6] Jing Guo, Supriyo Datta, Mark Lundstrom, and M P Anantam. Toward Multiscale Modeling of Carbon Nanotube Transistors. *International Journal for Multiscale Computational Engineering*, 2(2):257–276, 2004.

[7] Siyuranga O. Koswatta, Sayed Hasan, Mark S. Lundstrom, M. P. Anantram, and Dmitri E. Nikonov. Nonequilibrium Green's function treatment of phonon scattering in carbon-nanotube transistors. *IEEE Transactions on Electron Devices*, 54(9):2339–2351, sep 2007.

[8] Gordon E Moore. Chapter 7: Moore's Law at 40. In *Understanding Moore's Law: Four Decades of Innovation*, pages 67–84. 2006.

[9] Semiconductor Industry Association. 2015 International Technology Roadmap for Semiconductors (ITRS), Section 5: More Moore. 2015.

[10] Khalil Tamersit. Boosting the performance of an ultrascaled carbon nanotube junctionless tunnel field-effect transistor using an ungated region: NEGF simulation. *Journal of Computational Electronics*, 18(4):1222–1228, dec 2019.